NUMERICAL INVESTIGATION OF THE ENHANCED HEAT TRANSFER DUE TO CURVATURE–INDUCED LATERAL VORTICES IN LAMINAR FLOWS OVER SINUSOIDAL CORRUGATED-PLATE CHANNELS

Dr. Salam Hadi Hussain
University of Babylon/College of Engineering
Mechanical Engineering Department

Abstract

Single-phase air flow periodically developed at constant property (Pr=0.7), laminar forced convection in two-dimensional sinusoidal corrugated-plate channels, which are maintained at uniform wall temperature are considered. The governing differential equations for continuity, momentum, and energy equations are solved computationally using finite-volume technique, where the pressure term is handled by the SIMPLE algorithm. The computational grid is non-orthogonal and non-uniform, and it is generated algebraically. All the dependent variables are stored in a non-staggered manner. For the two-dimensional problem, numerical solutions are obtained for a wide range of channel corrugation aspect ratios ($0.25 \le \gamma \le 1.0$), plate spacing ratio ($0.25 \le \varepsilon \le 1.5$), and flow rates ($10 \le Re \le 1000$). The flow field is found to be strongly influenced by γ, ε and Re, and it displays two distinct regimes: a low Re or γ, ε undisturbed laminar-flow regime, and a high Re or γ, ε swirl-flow regime. In the no-swirl regime, the flow behavior is very similar to that in fully developed straight-duct flows with no cross-stream disturbance. In the swirl regime, flow separation and reattachment in the corrugation troughs generates transverse vortex cells that grow spatially with Re, γ and ε, and the transition to this regime also depends on Re, ε and γ. The mixing produced by these self-sustained transverse vortices is found to significantly enhance the heat transfer, depending upon Re, γ and ε, with a relatively small friction factor penalty.

Keywords: Finite volume; Convective heat transfer; Corrugated channel

دراسة عددية لزيادة معدل النقل الحراري الناجم من تكون الدوامات الجانبية لجريان طباقي في مجرى منحني على شكل موجة جيبية

د. سلام هادي حسين / مدرس
قسم الهندسة الميكانيكية / كلية الهندسة / جامعة بابل

الخلاصة

تم في هذا العمل دراسة جريان الهواء الأحادي الطور، المتناوب النمو، ذو الخصائص الثابتة (Pr= 0.7) في جريان الحمل القسري الطباقي الثنائي البعد في مجاري أو قنوات ذات شكل موجة جيبية عند درجات حرارة ثابتة للجدران . إن المعادلات الحاكمة للاستمرارية والزخم والطاقة تم حلها عددياً بأستخدام طريقة الحجوم المحددة حيث تمت معالجة مقدار الضغط بأستخدام الخوارزمية البسيطة (SIMPLE algorithm) مع استخدام شبكة غير متعامدة وغير متناسقة تولد جبرياً في ترتيب غير متناوب

لجميع المتغيرات الحاكمة ، تم إجراء حل عددي ثنائي البعد لمديات من نسبة التحايد للقناة المتموجة ($0.25 \le \gamma \le 1.0$) ونسبة المسافة الفاصلة للقناة ($0.25 \le \varepsilon \le 1.5$) ولمدى من أرقام رينولدز ($10 \le Re \le 1000$) . أظهرت نتائج الجريان الثنائي البعد تأثيرات كل من Re ، γ و ε على خواص الجريان ويمكن مشاهدة ذلك من خلال تكون منطقتين ، أحداهما منطقة طباقية غير متجانسة منخفضة القيم لكل من Re، γ و ε تسمى المنطقة الخالية من الدوامات الدورانية (No Swirl Regime) والأخرى منطقة الدوامات الدورانية (Swirl Regime) والتي تتكون عندما تكون قيم Re، γ و ε عالية ويكون سلوك الجريان في المنطقة الخالية من الدوامات الدورانية مشابه تماماً لجريان الهواء المتكامل النمو في المجاري المستقيمة إما في منطقة الدوامات الدورانية يمكن مشاهدة ظاهرة الانفصال وعودة الاتصال من خلال تكون دوامات مستعرضة أو متعاكسة تزداد بزيادة كل من Re ، γ و ε كما أن الانتقال من المنطقة الخالية من الدوامات الدورانية إلى منطقة الدوامات الدورانية يعتمد ايضاً على قيم Re، γ و ε. ان التداخل الحاصل بين الدوامات المستعرضة أو المتعاكسة يكون له الأثر الكبير في زيادة معدل انتقال الحرارة بالاعتماد على قيم Re، γ و ε مع وجود زيادة نسبية في معامل الاحتكاك.

Nomenclature:

Symbol	Description	Unit
a	Amplitude of wall waviness, **Figure 2(b1)**	mm
a_1, a_2	Transformation coefficients	
Br	Brinkman number $(=\rho \upsilon u_m^2 / k \Delta T)$	
c_p	Specific heat	J/kg K
d_h	Hydraulic diameter (=2S)	mm
f	Fanning friction factor based on projected flat-plate surface area, Eq. (16)	
H	Fin height, **Figure 2(b1)**	mm
k	Thermal conductivity	W/m K
j	Colburn factor (= Nu / Re $Pr^{1/3}$)	
J	Jacobean of transformation	
L	Pitch of fin waviness, **Figure 2(b)**	mm
Nu	Nusselt number based on projected flat-plate surface area, Eq. (14)	
Pe	Peclet number (= Re .Pr)	
Pr	Prandtl number (= μ c_p/k)	
q''_w	Wall heat flux	W/m^2
Re	Hydraulic-diameter-based Reynolds number (= u_m d_h /ν)	
S	Fin spacing, **Figure 2(b1)**	mm
S_ϕ	Source terms, Eq. (4)	
T	Temperature	K
U,V	Contravariant velocities	
u, v	Axial and lateral velocity components	m/s
x, y	Cartesian coordinates	
Greek symbols		
α	Flow cross-section aspect ratio (= S/H)	
ε	Channel spacing ratio (= S/2a)	
ϕ, Φ	Dependent variables (= U, V , and T, respectively)	
Γ	Dimensionless coefficient, Eqs. (4)-(5)	
γ	Cchannel corrugation ratio (=2a/L)	
ν	Dynamics viscosity	m^2/s
ρ	Density	kg/m^3
τ_w	Wall shear stress	N/m^2
ξ, η	Dimensionless body-fitted coordinates	
Subscripts		
b	Bulk or mixed-mean value	
i	Inlet conditions	
m	Mean or average value	

o	Outlet conditions
w	Wall conditions

Introduction:

Theoretical or experimental results for laminar flow heat transfer in complex and enhanced duct geometries are essential for the design and application of compact heat exchangers [1–3]. Often geometrically modified fins are incorporated, which, besides increasing the surface area density of the exchanger, also improve the convection heat transfer coefficient. Some examples of such enhanced surface compact cores include offset-strip fins, louvered fins, perforated fins, and corrugated or wavy fins [2–7]. Of these, sinusoidal wavy channels are particularly attractive for their simplicity of manufacture, potential for enhanced thermal–hydraulic performance, and ease of usage in both plate-fin and tube-fin type exchangers. Of particular interest for a wide spectrum of usage in food, pharmaceutical, and chemical processing is the plate heat exchanger (PHE) [8–10]. The corrugation patterns on the plate-surfaces of PHEs essentially promote enhanced heat transfer in their interpolate channels, thereby facilitating small approach temperature operation with a more compact heat exchanger. This is particularly beneficial for processing thermally degradable fluids such as food products, pharmaceutical media, personal care and biochemical products [9,10].

Typical sinusoidal wavy plate-fins are depicted in **Figure1(c),** and their geometric attributes are described by the waviness amplitude A, pitch L, inter-fin spacing S, and fin height H, as shown in **Figure2(*a*1).** Their dimensionless representation is given by the corrugation aspect ratio γ (=2A/L), fin spacing ratio ε (= S/2A), and flow cross-section aspect ratio α (= S/H).

Several investigations have addressed the issue of forced convective heat and/or mass transport in wavy or corrugated-wall channels used in a variety of different applications. These include wavy plate-fin channels [11–16], corrugated tube-fin cores [17–19], wavy-plate oxygenators [20–22], and corrugated inter-plate channels in plate-and-frame heat exchangers [23–27]. The surface corrugations in these devices have consisted of triangular, sinusoidal, and trapezoidal profiles, and the flow behavior has been studied both experimentally and computationally. It has generally been observed that wall corrugations induce a steady vortex or swirl in low Reynolds number flows in the trough regions of the wavy wall. This results in flow mixing and boundary layer disruption and thinning, thereby significantly enhancing the heat and mass transfer. The majority of computational models have considered a two-dimensional characterization of the flow geometry, which is valid when the fin height is much larger than the inter-fin spacing ($H >> S$ or $\alpha \rightarrow 0$; see **Figure 2(a1)).**

Nishmura et al. [20–22] have experimentally and numerically studied laminar flow mass transfer enhancement in two-dimensional wavy-plate channels by varying the pitch, amplitude, and the channel spacing in the range of $0.215 \leq \varepsilon \leq 1.33$ and $\gamma = 0.25$. Rush et al. [15] have experimentally investigate the flow behavior in wavy-plate channels with plate-spacing ratio $\varepsilon > 1.0$ and rather slender wall waviness ($0.1726 \leq \gamma \leq 0.208$), in an attempt to study the onset of flow mixing. In their finite-volume numerical analysis, Asako and Faghri [12], and Yang et al. [14] have considered periodically developed steady laminar flow and heat transfer in corrugated channels of a triangular profile with sharp and rounded corners, and with walls maintained at a constant temperature. Metwally and Manglik [25-26] have considered periodically developed laminar flow and heat transfer for Newtonian, power-law non-Newtonian, and Herschel-Bulkley fluids in wavy-plate channels with spacing ratio $\varepsilon = 1.0$, and corrugation aspect ratios in the range of $0.25 \leq \gamma \leq 1.0$. In these studies, the wall waviness is found to induce steady flow re-circulation or lateral vortices in the trough regions of the corrugated-plate channel. The strength of these vortices increases with Reynolds number and severity of wall waviness γ, leading to substantial heat transfer enhancement in comparison with flow in a flat parallel-plate channel; the associated friction loss also increases. As seen in the triangular-profiled wavy channel results of Comini et al. [19], this performance is also affected by the relative inter-plate spacing. A detailed understanding of the compound effects of wall-waviness aspect ratio γ and inter-plate spacing ε on the swirl flow

structure and its impact on forced convection is addressed in this paper, for the effective design and applications of sinusoidal wavy-plate fins.

The influence of the sinusoidal wavy-surface plate-fin geometry (γ and ε) on laminar airflow and convective heat transfer in the inter-fin channels is computationally investigated in this study. A two-dimensional flow geometry (H >> S, or α→0) is considered, and the role of inter-fin spacing and severity of wall waviness in promoting the wall-curvature-induced periodically developed steady swirl flows is highlighted. With plate surfaces maintained at a uniform temperature (UWT condition) for the heat transfer problem, which is representative of conditions in refrigeration-to-air or turbulent liquid flow liquid-to-air exchangers, a wide range of air (Pr = 0.7) flow rates in the low Reynolds number regime ($10 \le Re \le 1000$) are considered. The local velocity and temperature distributions are mapped, and the parametric variations in the average isothermal Fanning friction factor *f* and Colburn factor *j* results with γ, ε, and *Re* are outlined along with an assessment of the enhanced thermal–hydraulic performance.

Problem Formulation and Numerical Solution

For the sinusoidally corrugated parallel-plate channel geometry and reference coordinate system described in **Figure 2(a1),** constant property, periodically fully developed, steady laminar flows of viscous Newtonian fluids with heat transfer are considered. With in-phase wall waviness, the plate separation in the channel is twice the amplitude of the sinusoidal corrugation, i.e., valleys of the top-plate and peaks of the bottom-plate coincide on the mid-plane. The duct walls are maintained at a constant temperature (T or UWT boundary condition), and axial conduction (Pe >> 1) and viscous dissipation (Br << 1) are neglected. Thus, for the two-dimensional convection in the wavy channel, the governing equations for mass, momentum, and energy conservation can be expressed [29] as:

$$\frac{\partial u}{\partial x}+\frac{\partial v}{\partial y}=0 \qquad \text{.....(١)}$$

$$u\frac{\partial u}{\partial x}+v\frac{\partial u}{\partial y}=-\frac{1}{\rho}\frac{\partial p}{\partial x}+v\left(\frac{\partial^2 u}{\partial x^2}+\frac{\partial^2 u}{\partial y^2}\right)$$

$$u\frac{\partial v}{\partial x}+v\frac{\partial v}{\partial y}=-\frac{1}{\rho}\frac{\partial p}{\partial y}+u\left(\frac{\partial^2 v}{\partial x^2}+\frac{\partial^2 v}{\partial y^2}\right) \qquad \text{.....(٢)}$$

$$u\frac{\partial T}{\partial x}+v\frac{\partial T}{\partial y}=\alpha\left(\frac{\partial^2 T}{\partial x^2}+\frac{\partial^2 T}{\partial y^2}\right)$$

The above equations can be written in a general transport equation as :- .....(٣)

$$\frac{\partial(\rho u\phi)}{\partial x}+\frac{\partial(\rho v\phi)}{\partial y}=\frac{\partial}{\partial x}\left[\Gamma_\phi\left(\frac{\partial\phi}{\partial x}\right)\right]+\frac{\partial}{\partial y}\left[\Gamma_\phi\left(\frac{\partial\phi}{\partial y}\right)\right]+S_\phi$$

This equation serves as a starting point for computational procedure in (FVM) [Ferzinger et. al. (1999)][32]. The continuity equation can be obtained if ($\Phi=1$, $\Gamma_\Phi=0$ and $S_\Phi=0$), by setting ($\Phi=u$, v and $\Gamma_\Phi=\mu$, N-S equation can be obtain and energy equation can be obtained if ($\Phi=T$ and $\Gamma_\Phi=\mu/pr$). The two terms in the left of the general transport equation (Eq. 4) are convective terms, the first two terms in the right side of general transport equation (Eq. 4) are diffusive terms and the last term is the source term. For the general curvilinear coordinates system (ξ, η), the general transport equation (Eq. 4) can be transformed to the following form:- (ξ)

$$\frac{\partial}{\partial\xi}\left(\rho U\Phi-\frac{a_1\Gamma_\Phi}{J}\frac{\partial\Phi}{\partial\xi}\right)+\frac{\partial}{\partial\eta}\left(\rho V\Phi-\frac{a_2\Gamma_\Phi}{J}\frac{\partial\Phi}{\partial\eta}\right)=S_{NEW} \qquad \text{.....(5)}$$

where (U, V) are the contravariant velocity components and $S_{NEW}=JS_\Phi+S_N$ where S_N is the source term due to non orthogonal characteristic of grid system which disappear under orthogonal grid system. The transformation coefficients (a_1, a_2) are defined as:-

$$a_1 = \xi_x^2 + \xi_y^2$$
$$a_2 = \eta_x^2 + \eta_y^2 \qquad \text{…….(6)}$$

and the transformation metrics are calculated as follows :

$$\left.\begin{aligned} \xi_x &= \frac{y_\xi}{J} \\ \xi_y &= \frac{-x_\eta}{J} \\ \eta_x &= \frac{-y_\xi}{J} \\ \eta_y &= \frac{x_\xi}{J} \end{aligned}\right\} \qquad \text{…….(7)}$$

These are subject to the following no slip, uniform wall temperature, and periodicity boundary conditions, respectively:

The velocity on the wall equal to
zero i.e. u=v=0 at y= a sin(πx/L) and y=$2a$+a sin(πx/L) …….(8)

The temperature on the wall equal to
$T=T_w$ *at* $y=a\ sin(\pi x/L)$ and $y=2a+a\ sin(\pi x/L)$ …….(9)

To attain the fully developed flow in the stream wise direction, the following periodic boundary conditions are used for a wave of length 2 λ,

$$\left.\begin{aligned} u(x) &= u(x+L) \\ v(x) &= u(x+L) \\ (T/T_w)(x) &= (T/T_w)(x+L) \end{aligned}\right\} \qquad \text{…….(10)}$$

The flow and temperature fields were studied under the assumption of a fully developed flow, From the periodically a fully developed velocity distribution, on the basis of the velocity component tangential to the boundary and its derivative normal to the boundary (or the normalized gradient: $(\partial\phi/\partial n) = \nabla\phi \cdot \hat{n}$ the local wall shear stress can then be calculated from

$$\tau_{w,x} = -\mu\left[1 + (\pi L/2)^2 \cos^2(\pi x/L)\right]^{-1} (\partial u/\partial y) \qquad \text{…….(11)}$$

Likewise, the local wall heat flux is given by

$$q''_{w,x} = -k\left[1 + (\pi L/2)^2 \cos^2(\pi x/L)\right]^{-1/2} (\partial T/\partial y) \qquad \text{…….(12)}$$

The average flow velocity u_m and the bulk-mean temperature T_m are, respectively, obtained from their standard definitions as:

$$\left.\begin{aligned} u_m &= \frac{1}{2a}\int_0^{2a} u\,dy \\ T_m &= \frac{1}{(2au_m)}\int_0^{2a} uT\,dy \end{aligned}\right\} \qquad \text{……..(13)}$$

The overall Nusselt number is computed from the temperature field by applying the energy balance over the one-period flow domain, and the log-mean temperature difference (LMTD) as

$$Nu = \frac{\dot{m}_{air} cp(T_{b,out} - T_{b,in}) D_h}{kA_h (LMTD)} \quad \text{.....(14)}$$

Where

$$LMTD = \frac{(T_w - T_{b,out}) - (T_w - T_{b,in})}{\ln[(T_w - T_{b,out})/(T_w - T_{b,in})]} \quad \text{.....(15)}$$

the average friction factor is given:

$$f_{avg} = \frac{2\Delta p * D_h}{\rho L u_m^2} \quad \text{.....(16)}$$

where k is the thermal conductivity of air. Reynolds number based on the hydraulic diameter, D_h, of the channel as follows:

$$\mathrm{Re} = \frac{u_m D_h}{\nu} \quad \text{..... (17)}$$

To determine the flow dynamic field, a simulation by a fluid dynamic calculation (C. F. D.) has been used. Eq.(5) is discretizated according to the Patankar procedure [29]. The discretization in finite volume employed uses an integral form of the general Eq.(5); the calculation domain is subdivided in a set of small elementary control volumes (or cells) on which the integration is applied. Finally this discretization produces an algebraic equation system. To obtain numerical solutions, the governing differential equations were discretized on a structured, non-orthogonal grid using the finite-volume method. A typical computational mesh for the flow geometry is shown in Figure (3), where the grid is uniform in the axial x or ξ direction, but non-uniform in the lateral y or η direction. The latter non-uniform mesh distribution is controlled by the following function:

$$\eta = ay_1 + \frac{(1-a)(1-\tanh[b(1-y_1)])}{\tanh(b)} \quad \text{.....(18)}$$

Here y_1 has a uniform distribution in the range $0 \le y_1 \le 1$, and the η distribution in the range $0 \le \eta \le 1$ is controlled by the two constraints a and b that were set as $a = 0.1$ and $b = 2.0$ in all simulations. This ensures a denser mesh near the walls for properly treating the high velocity and temperature gradients. Both the diffusion and convection terms are treated by the power-law differencing scheme, and the source terms by central differencing. The SIMPLE algorithm was applied to evaluate the coupling between the pressure and velocity [29].

The convergence criterion for all calculations, represented by the relative magnitude of the error, was grouped, respectively by velocity fields, pressure and temperature by the following relation:

$$error = \left| \frac{\Phi_{new} - \Phi_{old}}{\Phi_{new}} \right| \langle 10^{-5} \quad \text{.....(19)}$$

Φ represents the axial and transversal components of the velocity, pressure and temperature. The computer program which is preparing and writing with FORTRAN 90 language in the present work embodies subroutines for solving the equations U, V, P, and T receptively.

Validation of Numerical Results

The numerical results were first validated with analytical solutions for a parallel-plate flow channel, which is obtained by setting the amplitude A = 0 in the simulation. The computed values of $f = 24.0679/Re$ and Nu = 7.654 were within 0.282 % & 1.4 % of the exact analytical results of

24 and 7.541 respectively [30]. To determine the proper grid size required for numerical simulation, grid refinement experiments were performed. As an illustrative example, for the case of *Re* =250, γ = 0.25, and ε =1.0, the *f* and *j* results for five different mesh sizes are listed in **Table 1**. It can be seen from the results that the values of the friction factor (*f*) and Colburn factor (*j*), obtained at different grids, vary by less than 1 %, thus demonstrating the adequacy of the grid adopted and the numerical accuracy of the method.

Results and Discussion

Numerical results for the velocity and temperature fields, isothermal Fanning friction factor, Colburn factor, and their variation with flow Reynolds number in different wavy-plate channels (ε = 0.25, 0.5, 0.75, 1.0, 1.5), and (γ = 0.25, 0.5, 0.75, 1.0) are presented. The simulation results show the change of flow pattern with flow rates and channel geometries. The influence of the flow geometry on the local velocity and temperature distribution, and the nature of wavy-surface-induced lateral vortex structure are delineated, along with an evaluation of the enhanced thermal–hydraulic performance.

Velocity field and temperature distribution in a straight and typical wavy flow channel with geometry parameter ε = 1.0 and γ = 0.5 at flow rate Re = 350 is shown in **Figure 4(A).** The velocity streamlines distribution and isotherm map distribution in recirculation region are shown in **Figure 4(B)** and **(C)** respectively. Lateral vortex is clearly seen in the wavy flow channel, and it is one of the basic flow characteristic in wavy flow channel at high flow rate condition.

The onset, development, and growth of steady lateral vortices or re-circulation in the troughs of wavy plate-fin channels with changing flow rates are depicted in **Figure (5).** Streamlines for flows with Re = 10, 100, 500, and 1000 in three different wavy-fin geometries with ε = 1.0, and γ = 0.25, 0.5, 75, and 1.0 are graphed, and the strong influences of Re and severity of wall waviness γ are clearly evident. With increasing flow rates, wall-curvature- induced effects manifest in fluid separation downstream of the wavy-surface peak, with reattachment upstream of the subsequent peak, and the consequent development of re-circulating cells in the valley regions. This lateral vortex is triggered at a lower flow rate in channels with more severe wall waviness (Re ~ 100 with γ = 0.5, as compared to Re > 100 with γ = 0.25; ε = 1.0 in both cases). Also, the extant of the lateral swirl flow area coverage increases with Re and γ. At very low flow rates (Re ~ 10), however, viscous forces dominate to produce undisturbed streamline flows and swirl is not developed, irrespective of the wall-corrugation aspect ratio γ.

The corresponding impact on the local convective temperature distribution in air (Pr = 0.7) flows between uniform temperature plates is illustrated by the isotherm plots of **Figure (6).** With the onset of trough-region recirculation, there is considerable thinning of the boundary layer and the flow field exhibits regions of thermal mixing. Also, the increasing spatial coverage of the trough vortices with Re and γ results more uniform core region temperature distributions, and much sharper wall temperature gradients.

That the inter-plate-fin spacing, represented by the dimensionless ε (= $S/2a$), significantly influences the development of re-circulating flows in the wavy-wall valleys is seen from the stream lines graphed in **Figure (7).** The flow fields at Re = 10, 100, 500, and 1000 in channels with γ = 1.0, and $0.25 \le \varepsilon \le 1.5$ are depicted. With increasing Re and/or plate spacing ε, the lateral vortex in the trough tends to grow and envelop much of the core flow region, thereby promoting flow mixing and increased momentum transport. As the plate separation decreases ($\varepsilon \rightarrow 0.5$), viscous effects suppress swirl and undisturbed streamline flows prevail that follow the channel-wall contours. This flow behavior, however, depends on both ε and Re for any given γ.

Similarly, the air flow (Pr = 0.7) temperature distribution reflects a fully developed duct flow like condition when ε is small, as seen in **Figure (8).** With increasing ε or Re and the attendant development of lateral vortices, on the other hand, the temperature field displays a periodicity that is characterized by local regions of considerably thin thermal boundary layers, resulting in the local

heat transfer performance enhancement. The temperature distribution in the channel core becomes more uniform with the growth of swirl, and the overall convection heat transfer increases.

The effects of the duct geometry (as described by γ) on the flow frictional losses are seen in **Figure (9),** where results for the change in Fanning friction factor *f* with Re are graphed for γ = 0.25, 0.375, 0.5, 0.75, and 1.0. The well-known result for flow in a flat parallel-plate channel ($f = 24/Re$), which corresponds to fully developed laminar flow in the reference case of $\gamma = 0$ is also included. The increasing friction factor behavior with increasing severity of the plate corrugation ($\gamma > 0 \rightarrow 1$) is clearly evident. Also it can be seen that the influence of the onset of swirl flow in the troughs of the wall corrugation on *f*, which is depicted by the deviation from the log-linear behavior of *f*-Re at higher Reynolds number in each γ case. As pointed out earlier, the increased friction factor in this regime is predominantly due to the onset and growth of the lateral vortices in the channel troughs that enhance fluid momentum transfer thereby increasing the wall shear stress. In the low Reynolds number regime, however, where (*f*-Re) is constant, the increase in the frictional loss with γ is primarily due to the increased effective flow length or surface area. The interplay of channel plate surface geometry and flow distribution, which is also reflected in the friction factor results, clearly indicates that the flow can be categorized into two distinct regimes: an undisturbed laminar flow regime, and a steady swirl-flow regime characterized by self-sustained transverse vortices in the wall trough regions. This demarcation is graphically shown in the *f*-Re results of **Figure (9).** A general critical Reynolds number, however, does not uniquely represent the transition from one regime to the other, and it is different for each channel of different corrugation aspect ratio γ.

That the transverse vortices induced in the troughs of the plate surface corrugations promote enhanced convection in the flow cross section and increase the heat transfer coefficient is evident from **Figure (10).** In this figure, the variation in Nusselt number with Reynolds number for airflow (Pr = 0.7) and different corrugation aspect ratio (γ) is presented. Relative to the performance of the parallel-plate channel in fully developed laminar flow (Nu = 7.541), the heat transfer coefficient in corrugated channels is enhanced several folds, depending upon γ and Re. The largest increasing in the period-averaged Nusselt number is obtained with high γ and Re, where, for example, with γ = 1.0 and Re = 1000 the Nusslet number is 5.335 times higher than that in a parallel-plate channel. Furthermore, similar to the *f*-Re behavior seen in **Figure (9)**, the effect of swirl distribution diminishes as Re and/or γ decreases.

The concomitant influence of the altered flow structure in wavy-plate ducts on the period-averaged heat transfer coefficient is depicted in **Figure (11),** where the variations in the Colburn *j* factors with Re, γ, and ε are presented for air flows (Pr = 0.7). Included is the result for fully developed laminar flow in a flat-plate channel given by Nu = 7.541 (j x Re = 8.493 and Pr = 0.7) for the constant wall temperature condition. In the presence of the wall- trough region lateral swirl and the associated improvement in fluid convection, the overall heat transfer coefficient is seen to enhance significantly with increasing γ and ε in the Re > 100 regime. In the low flow rate (Re ~ O [10]) regime, just as its frictional loss counterpart, j x Re is also constant and the heat transfer enhancement is mainly due to the increased effective surface area and larger residence time provided by the corrugated channel. Again, the combined interplay of γ, ε and Re is similar to that seen in the friction factor results.

Conclusions:

Laminar air flow (Pr = 0.7) and forced convection heat transfer in two-dimensional wavy plate-fin channels has been computationally simulated. Constant property, and periodically developed fluid flow and heat transfer are considered. The steady-state governing equations (continuity, momentum, and energy equations) were solved using finite-volume technique, and the SIMPLE algorithm was used to couple the pressure-velocity fields. Periodic boundary conditions were applied to the solution domain, and the effects of thermal and hydraulic entry lengths were

neglected. The 2-D simulations were conducted for flow channels with following geometric parameters: $0.25 \le \gamma \le 1.0$, and $0.25 \le \varepsilon \le 1.5$. The following conclusions can be drawn from the results of the present work :

1. The computational results presented in this study provide a detailed understanding of the air flow (Pr = 0.7) forced convection behavior in wavy plate- fin channels in the low Reynolds number regime ($10 \le Re \le 1000$).
2. The results show that the wavy-wall curvature induces lateral vortices in the trough region, which grow in magnitude and spatial flow coverage with increasing Re and ε or γ.
3. The inter-plate separation, however, is critical for the development of this flow structure. With small separation ($\varepsilon \le 0.5$), viscous forces dominate and a streamline, fully developed flow type behavior prevails.
4. With large inter-plate gap ($\varepsilon = 1.0$), this effect diminishes and the boundary layer separation gives rise to a vortex flow structure in the wall waviness valley region.
5. The recirculation is enveloped in the near-wall axial flow separation bubble, and its spatial growth is governed by Re, γ, and ε.

References

[1] Webb, R.L., "Principles of Enhanced Heat Transfer", Wiley, New York, 1994.

[2] Bergles, A.E., " Techniques to enhance heat transfer", in: W.M. Rohsenow, J.P. Hartnett, Y.I. Cho (Eds.), "Handbook of Heat Transfer", third ed., McGraw-Hill, New York, 1998 (Chapter 11).

[3] R.M. Manglik, "Heat transfer enhancement", in: A. Bejan, A.D. Kraus (Eds.), "Heat Transfer Handbook", Wiley, New York, 2003 (Chapter 14).

[4] Kays, W.M. , London, A.L., "Compact Heat Exchangers", third ed., McGraw-Hill, New York, 1984.

[5] Manglik, R.M. , Bergles, A.E., "Heat transfer and pressure drop correlations for the rectangular offset-strip-fin compact heat exchanger", Exp. Therm. Fluid Sci. 10 (2) (1995) pp:171–180.

[6] Webb, R.L. ,"Principles of Enhanced Heat Transfer", Wiley, New York, 1994.

[7] Shah, R.K., "Heat exchangers", in: W.M. Rohsenow, J.P. Hartnett, Y.I. Cho (Eds.), "Handbook of Heat Transfer", McGraw-Hill, New York, 1998 (Chapter 17).

[8] Shah, R.K., and Focke, W.W., "Plate heat exchangers and their design theory", in: R.K. Shah, E.C. Subbarao, R.A. Mashelkar (Eds.), "Heat Transfer Equipment Design", Hemisphere, New York, 1988, pp: 227–254.

[9] Manglik, R.M., "Plate heat exchangers for process industry applications: Enhanced thermal-hydraulic characteristics of chevron-plates", in: R.M. Manglik, A.D. Kraus (Eds.), Process, " Enhanced and Multiphase Heat Transfer", Begell House, New York, 1996, pp: 267–276.

[10] Wang, L., Sunden, B., Manglik, R.M., "Plate Heat Exchangers: Design, Applications, and Performance, W.I.T. Press, Southampton, UK, in press.

[11] Vajravelu, K., "Fluid flow and heat transfer in horizontal wavy channels", Acta Mech. 35 (1980) pp:245–258.

[12] Asako, Y. and Faghri, M., " Finite-volume solutions for laminar flow and heat transfer in a corrugated duct", J. Heat Transfer 109 (3) (1987), pp:627–634.

[13] Garg, V.K., and Maji, P.K.,"Flow and heat transfer in a sinusoidally curved channel", Int. J. Eng. Fluid Mech. 1 (3) (1988), pp:293–319.

[14] Yang, L.C., Asako, Y., Yamaguchi, Y., and Faghri, M., "Numerical predication of transitional characteristics of flow and heat transfer in a corrugated duct", J. Heat Transfer 119 (1) (1997), pp: 62–69.

[15] Rush, T.A. , Newell, T.A. , and Jacobi, A.M., "An experimental study of flow and heat transfer in sinusoidal wavy passages", Int. J. Heat Mass Transfer 42 (1999), pp: 1541–1553.

[16] Zhang, J., Manglik, R.M., Muley, A., and Borghese, J.B., "Three-dimensional numerical simulation of laminar air flows in wavy plate-fin channels", in: Proceedings of 13th International Symposium on Transport Phenomena (ISTP –13), Victoria, BC, Canada, July, pp:14–18, 2002.

[17] Min, J. and Webb, R.L., "Numerical predications of wavy fin coil performance", J. Enhanced Heat Transfer 8 (3) (2001), pp:159– 173.

[18] Comini, G., Nonino, C., and Savino, S., "Convective heat and mass transfer in wavy finned-tube exchangers", Int. J. Numer. Methods Heat Fluid Flow 12 (2) (2002), pp:735–755.

[19] Comini, G., Nonino, C., and Savino, S., "Effect of space ratio and corrugation angle on convection enhancement in wavy channels", Int. J. Numer. Methods Heat Fluid Flow 13 (4) (2003), pp: 500–519.

[20] Nishimura, T., Ohori, Y., Kajimoto, Y., and Kawamura, Y., "Mass transfer characteristics in a channel with symmetric wavy wall for steady flow", J. Chem. Eng. Jpn. 18 (6) (1985), pp:550–555.

[21] Nishimura, T., Kajimoto, Y., and Kawamura, Y.,"Mass transfer enhancement in channels with a wavy wall", J. Chem. Eng. Jpn. 19 (2) (1986), pp:142–144.

[22] Nishimura, T., Murakami, S., Arakawa, S., and Kawamura, Y., "Flow observation and mass transfer characteristics in symmetrical wavy-walled channels at moderate Reynolds number for steady flow", Int. J. Heat Mass Transfer 33 (5) (1990), pp:835–845.

[23] Focke, W.W. , Zachariades, J., and Olivier, I., "The effect of the corrugation inclination angle on the thermo-hydraulic performance of plate heat exchangers", Int. J. Heat Mass Transfer 28 (8) (1985), pp: 1469–1479.

[24] Bereiziat, D., Devienne, R., and Lebouche, M., "Local flow structure for non-Newtonian fluids in a periodically corrugated wall channel", J. Enhanced Heat Transfer 2 (1–2) (1995), pp:71–77.

[25] Metwally, H.M., and Manglik, R.M., "Numerical solutions for periodically-developed laminar flow and heat transfer in sinusoidal corrugated plate channels with constant wall

temperature", in: Proceedings of 2000 National Heat Transfer Conference, Paper No. NHTC2000-12216, ASME, New York, 2000.

[26] Metwally, H.M., and Manglik, R.M., "A computational study of enhanced heat transfer in laminar flows of non-Newtonian fluids in corrugated-plate channels", in: R.M. Manglik, T.S. Ravigururajan, A. Muley, R.A. Papar, J. Kim (Eds.), "Advances in Enhanced Heat Transfer", HTD-vol. 365/PIDvol. 4, ASME, New York, 2000, pp: 41–48.

[27] Zimmerer, C., Gschwind, P., Gaiser, G., and Kottke, V., "Comparison of heat and mass transfer in different heat exchanger geometries with corrugated walls", Exp. Therm. Fluid Sci. 26 (2002), pp: 269–273.

[28] Patankar, S.V., Liu, C.H., and Sparrow, E.M., "Fully developed flow and heat transfer in ducts having streamwise-periodic variations of cross-sectional area", J. Heat Transfer 99 (1977), pp:180–186.

[29] Patankar, S.V., "Numerical heat transfer and fluid flow", Hemisphere Publishing Corporation, New York, 1980.

[30] John, H., Lienhard, I.V., John, H., and Lienhard, V., "A Heat Transfer Textbook", Publishing by Phlogiston Press Cambridge, U.S.A., 2005.

[31] Zhang J., Kundu J., and Manglik, R. M., "Effect of fin waviness and spacing on the lateral vortex structure and laminar heat transfer in wavy-plate-fin cores", Int. J. Heat Mass Transfer 47 (2004), pp: 2283–2292.

[32] Ferzinger, J. and Peric, M., "Computational methods for fluid dynamics", 2nd edition Springer Verlag, Berlin Hedelberg, 1999.

Table 1: Effect of grid refinement on *f* and *j* in a typical wavy-plate channel With γ = 0.25, and ε =1.0 for flow with *Re* = 250

Grid size (ξ x η)	Friction factor *f*			Colburn factor *j*		
	Present work	Jiehai et al. [31]	deviation %	Present work	Jiehai et al. [31]	deviation %
50 x 25	0.13556	0.13702	0.065	0.052328	0.052139	0.36
60 x 35	0.13787	0.13879	0.660	0.052899	0.052737	0.30
80 x 45	0.13952	0.13922	0.210	0.053066	0.053018	0.90
100 x 55	0.14015	0.13988	0.190	0.053188	0.053124	0.12
120 x 65	0.14121	0.13997	0.880	0.053198	0.053167	0.05

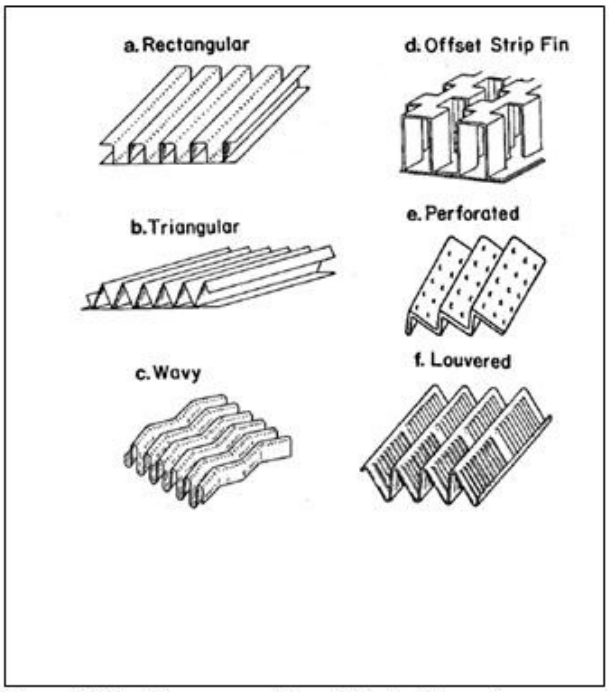

Figure(1) Surface geometries of plate- fin exchanger : (a) rectangular , (b) triangular, (c) Wavy-plate fins, (d) offset strip fin (e) perforated and (f) louvered.

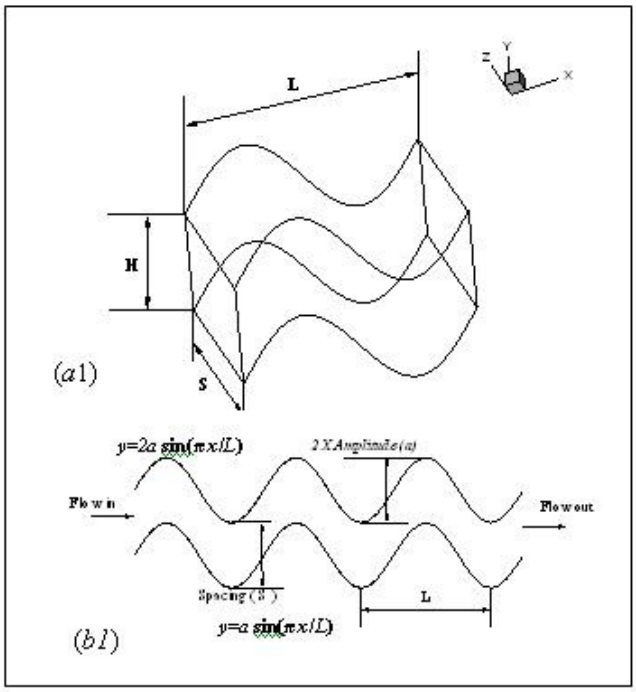

Figure (2) typical sinusoidally corrugated plate fins (*a*1), geometrical description and a two-dimensional representation of the inter-fin flow channel (*b*1)

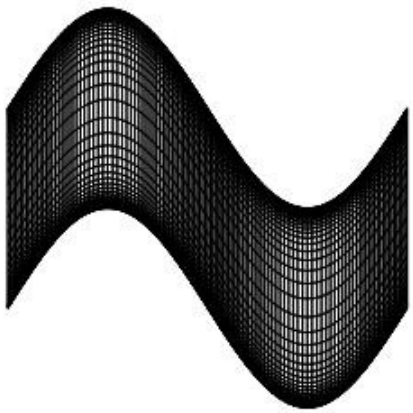

Figure (3) Computational Representation of Two-Dimensional In The Wavy Flow Channel With Non-Uniform and Non-Orthogonal Grid.

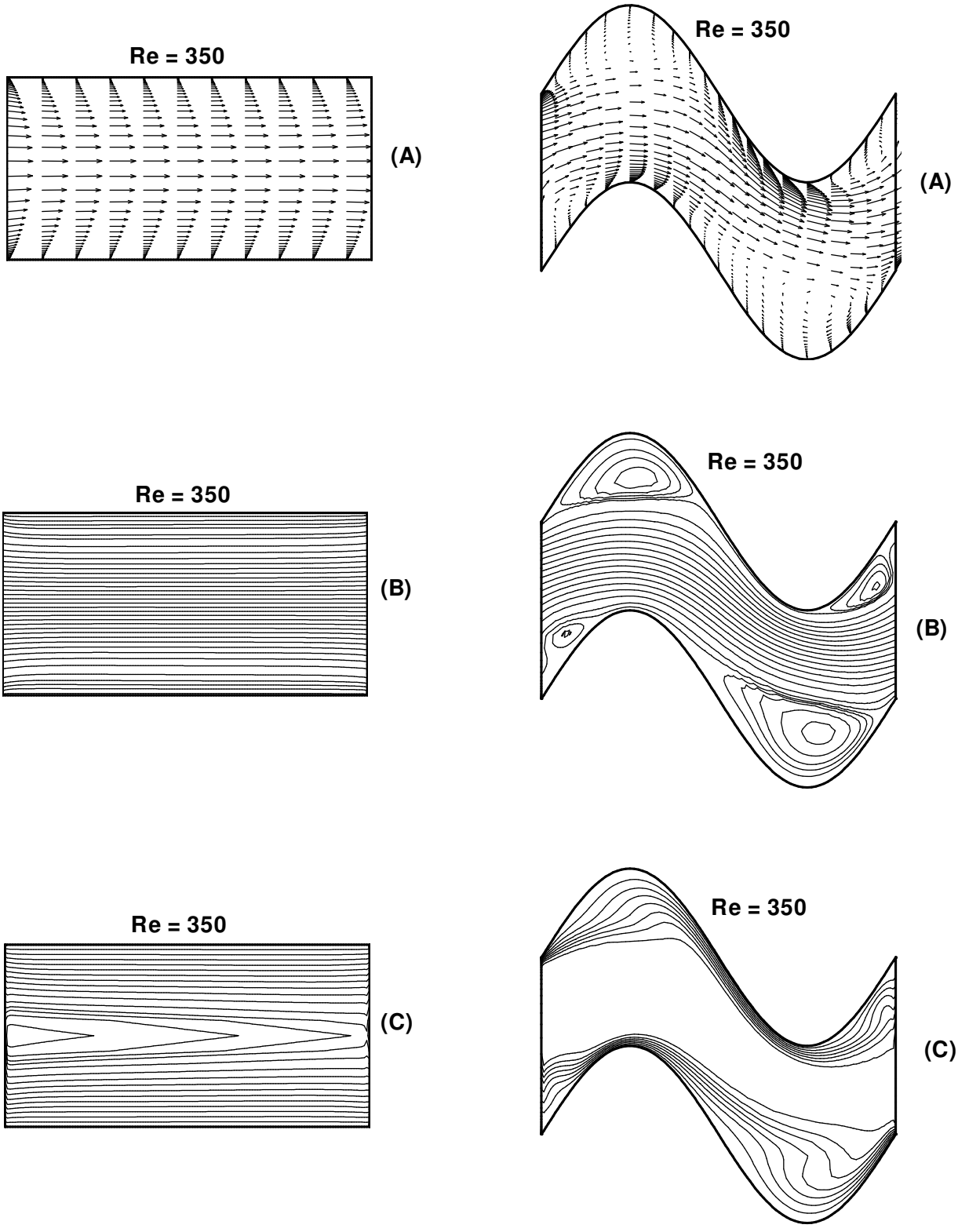

Figure (4) Velocity and temperature field in the straight flow channel (left) and wavy flow channel (ε = 1.0 and γ = 0.5) (right) at Re = 350, (A) overall velocity vector, (B) overall streamlines, and (C) overall isotherm map.

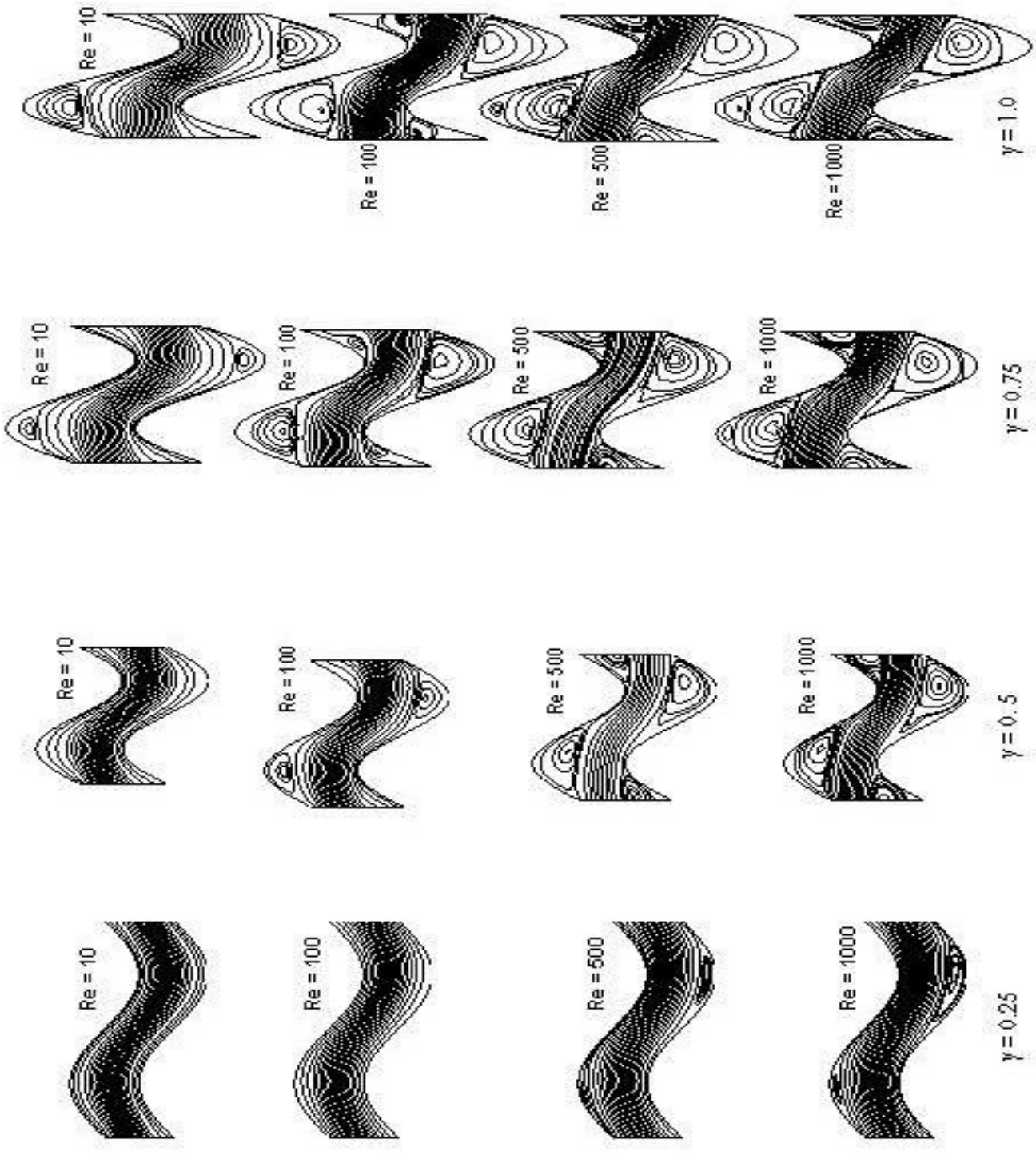

Figure (5) Streamline distributions for air (Pr = 0.7) flows in wavy-plate channels with relative spacing of ε = 1.0 but different corrugation aspect ratio γ (0.25, 0.5, 0.75 and 1.0) and flow Reynolds numbers.

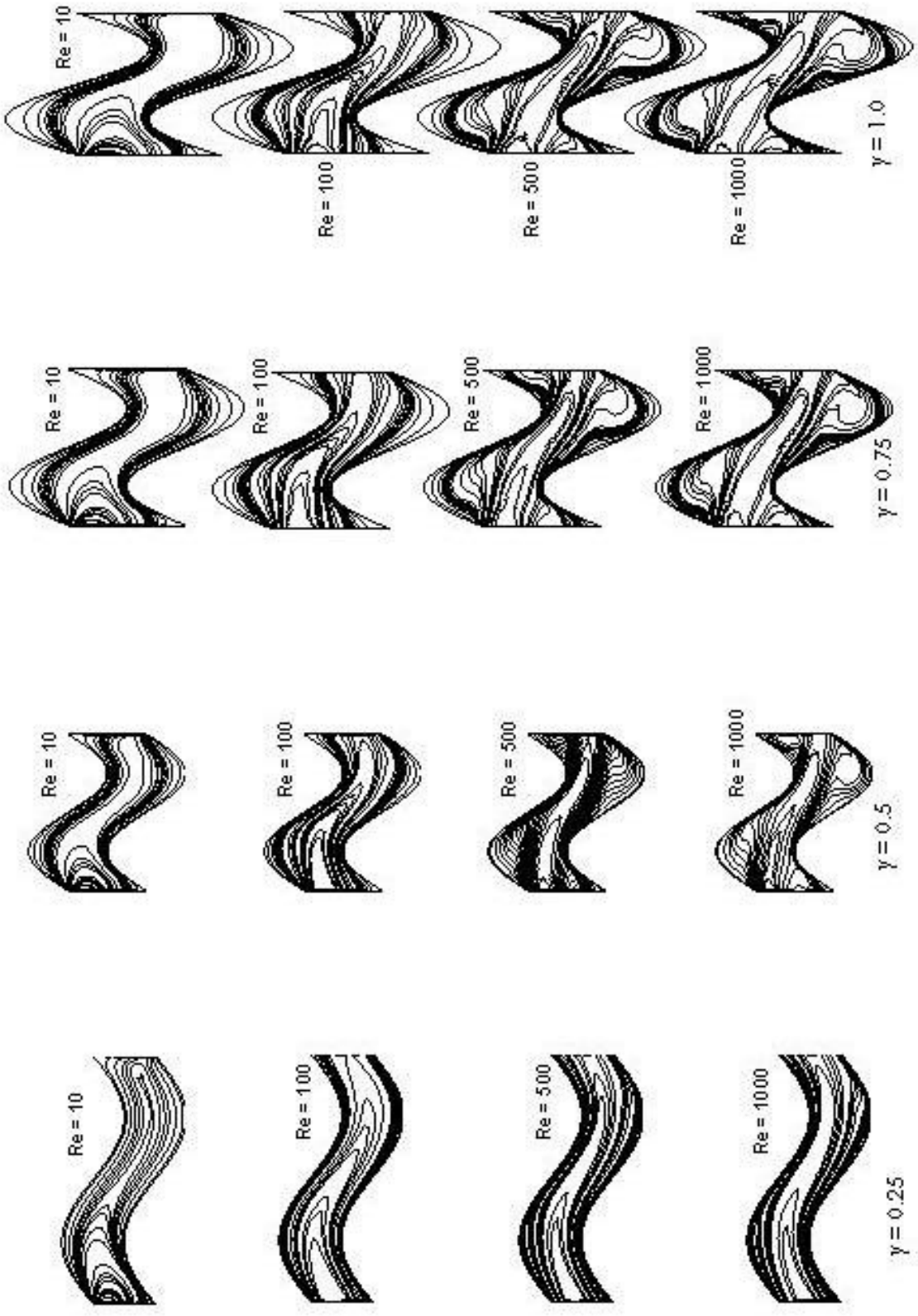

Figure (6) Isotherm maps for air (Pr = 0.7) flows in wavy-plate channels with relative spacing of ε = 1.0 but different corrugation aspect ratio γ (0.25, 0.5, 0.75 and 1.0) and flow Reynolds numbers.

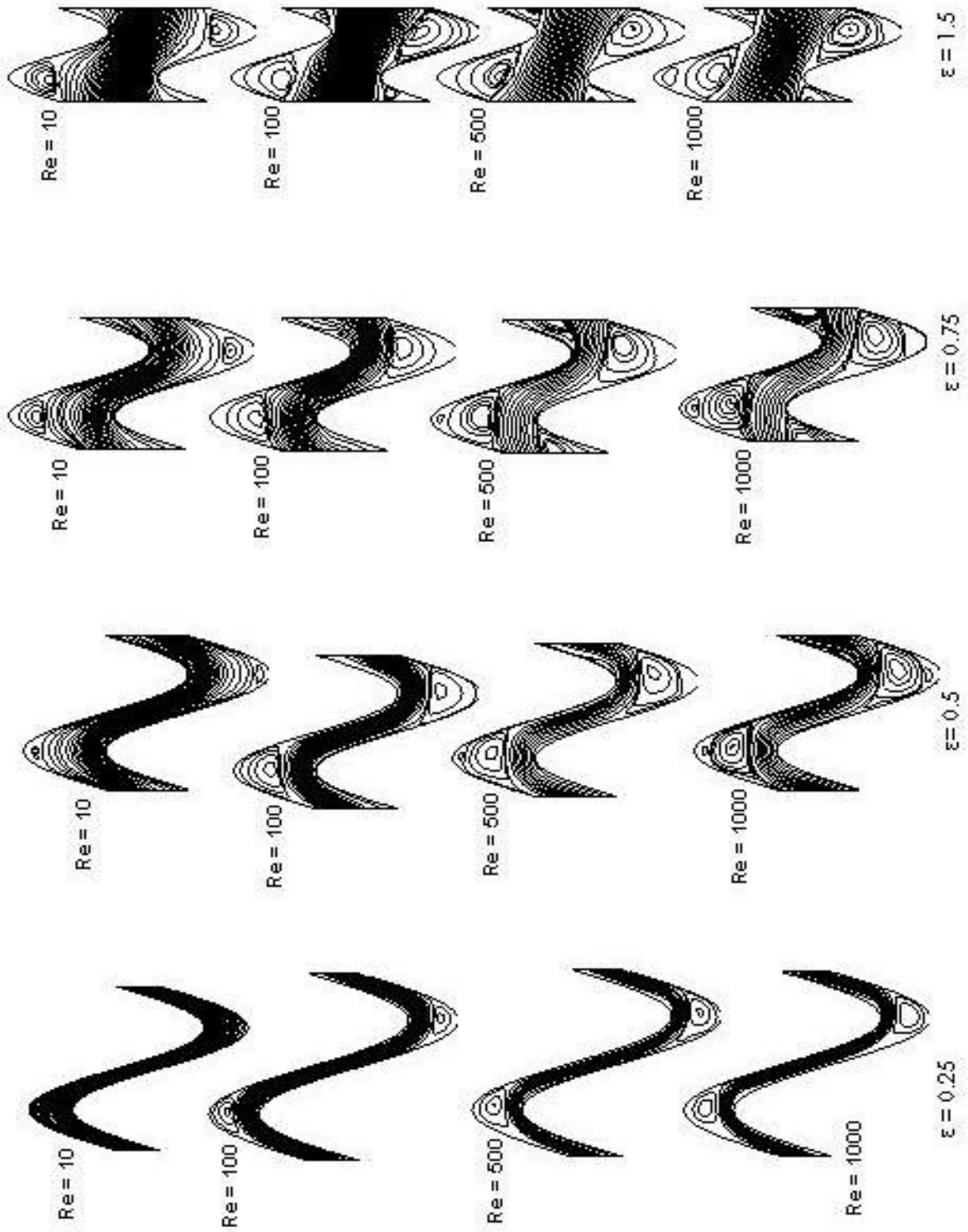

Figure (7) Streamline distributions for air (Pr = 0.7) flows in wavy-plate channels with corrugation aspect ratio γ = 1.0 but different relative spacing of ε (0.25, 0.5, 0.75 and 1.5) and flow Reynolds numbers.

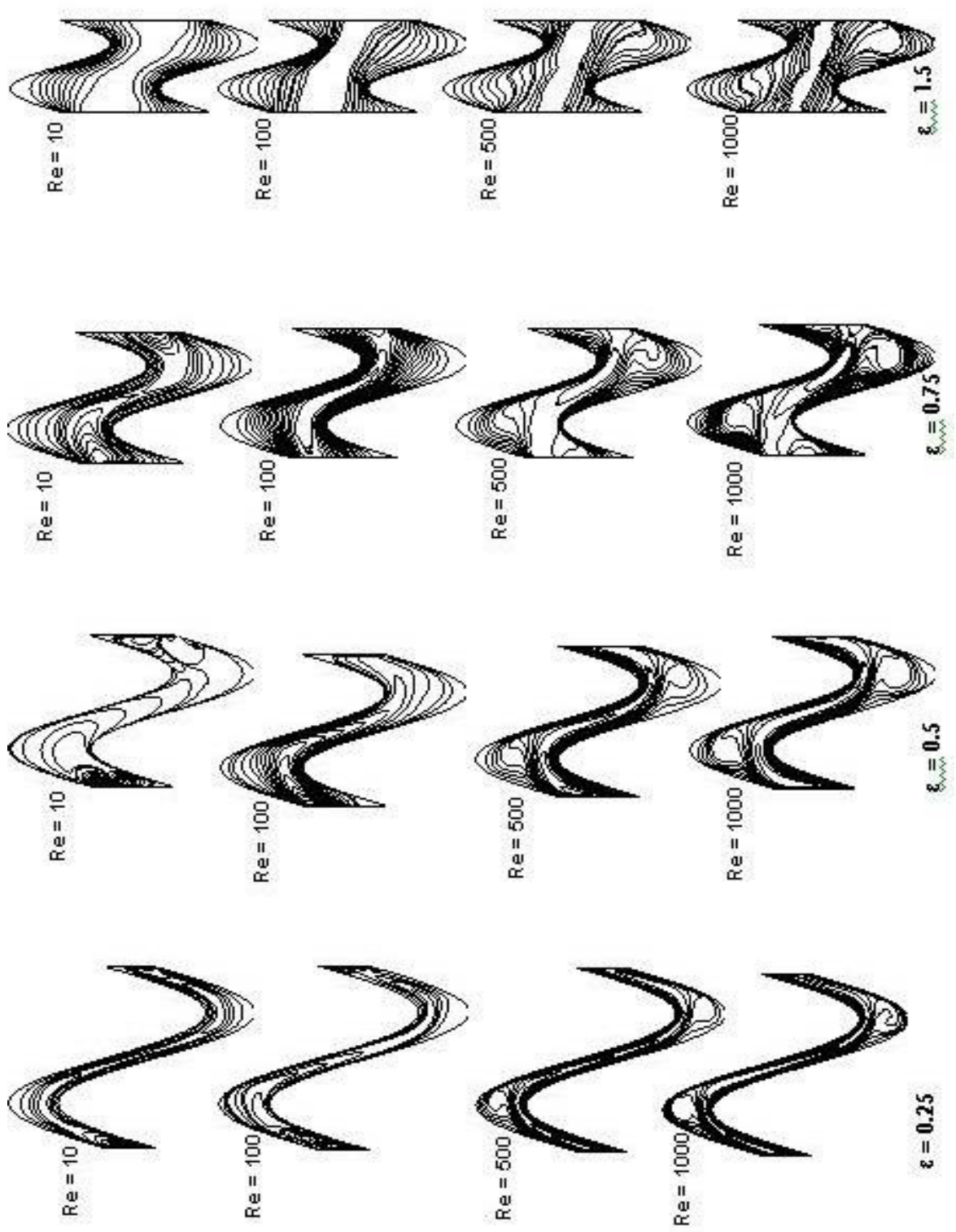

Figure (8) Isotherm maps for air (Pr = 0.7) flows in wavy-plate channels with corrugation aspect ratio $\gamma = 1.0$ but different relative spacing of ε (0.25, 0.5, 0.75 and 1.5) and flow Reynolds numbers.

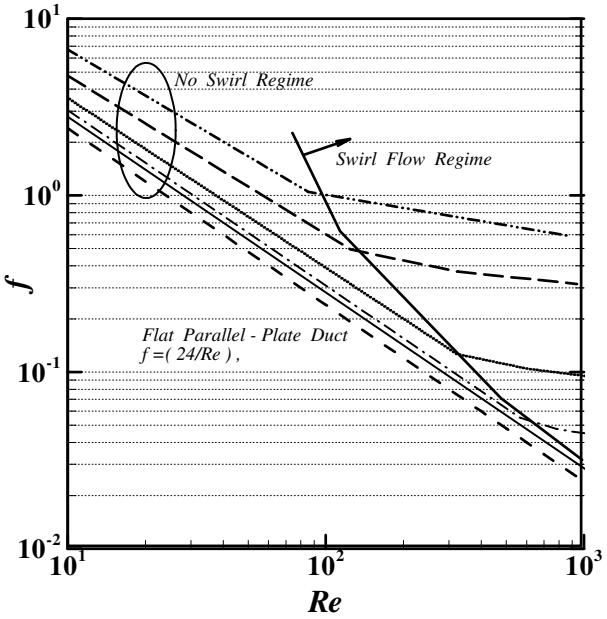

Figure (9) Isothermal Fanning friction factors for periodically developed laminar airflows in sinusoidal wavy-plate channels and channel spacing ratio ε = 1.0

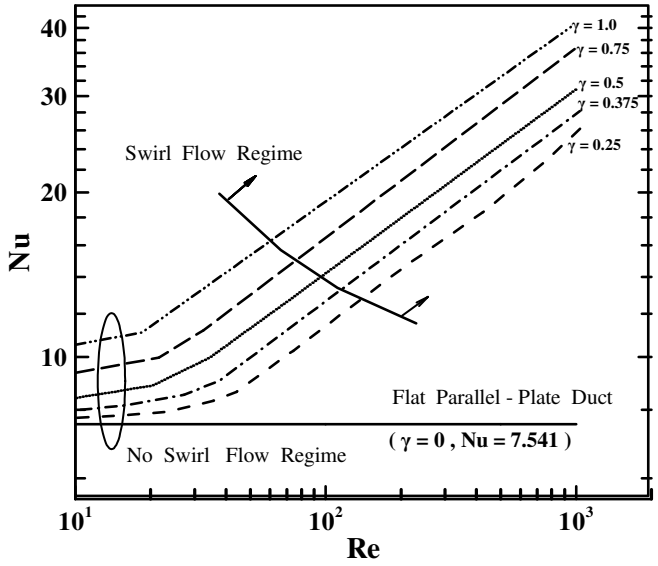

Figure (10) Periodically developed laminar airflows (Pr = 0.7) Nusselt numbers in sinusoidally corrugated parallel-plate channels with uniform wall temperature and channel

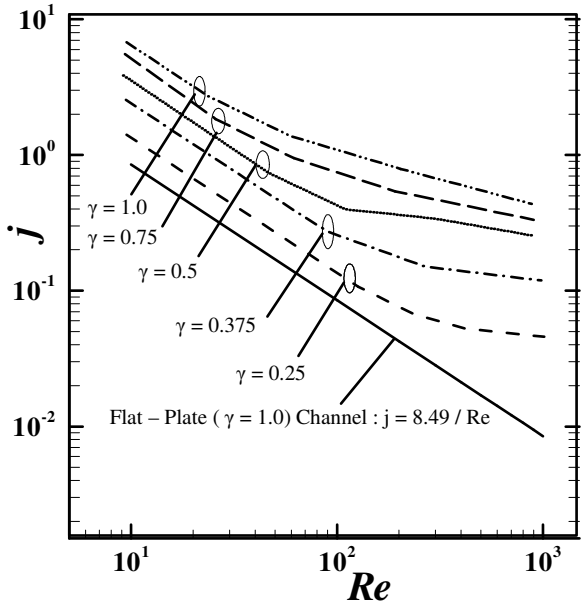

Figure (11) Colburn factors for periodically developed laminar airflows in sinusoidal wavy-plate channels with constant wall temperature and channel spacing ratio ε = 1.0

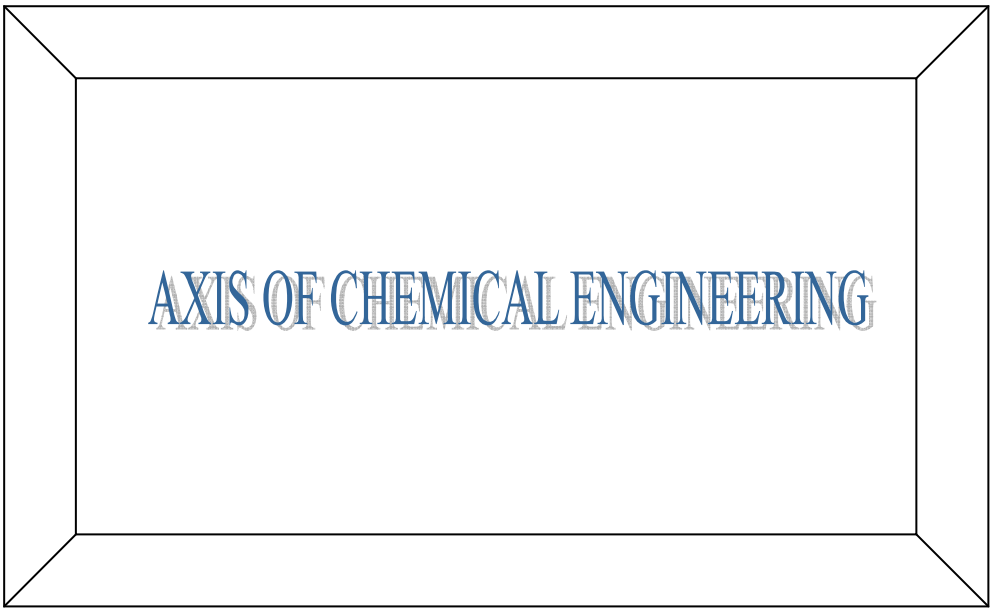
AXIS OF CHEMICAL ENGINEERING